Electronic Supplementary Material (ESI) for Journal of Materials Chemistry C.

Supporting information for

Superconductivity and structural instability in layered BiS_2-based $LaO_{1-x}BiS_2$

Yongliang Chen,‡*[ab] Yajing Cui,‡[a] Anh Pham,[bc] Yu Wang,[d] Mohan M. Bhadbhade,[d] Ruilong Wang,[a] Yufeng Su,[a] Hailong Hu,[b] Zhiwei Wen,[a] Cuihua Cheng,[a] Thiam Teck Tan,[b] Sean Li[b] and Yong Zhao*[ae]

a. *Key Laboratory of Magnetic Suspension Technology and Maglev Vehicle, Ministry of Education, and Superconductivity and New Energy R&D Center, Southwest Jiaotong University (SWJTU), Chengdu 610031, China.*

b. *School of Materials Science and Engineering, University of New South Wales (UNSW), Sydney, NSW 2052, Australia*

c. *Center for Nanophase Materials Sciences, Oak Ridge National Laboratory, Oak Ridge, TN 37830, USA*

d. *Solid State and Elemental Analysis Unit, Mark Wainwright Analytical Centre, University of New South Wales (UNSW), Sydney, NSW 2052, Australia*

e. *College of Physics and Energy, Fujian Normal University, Fuzhou, Fujian 350117, China*

‡ **Yongliang Chen and Yajing Cui contributed equally.**

E-Mail: llchen@home.swjtu.edu.cn, yzhao@home.swjtu.edu.cn

Supplementary figures and table

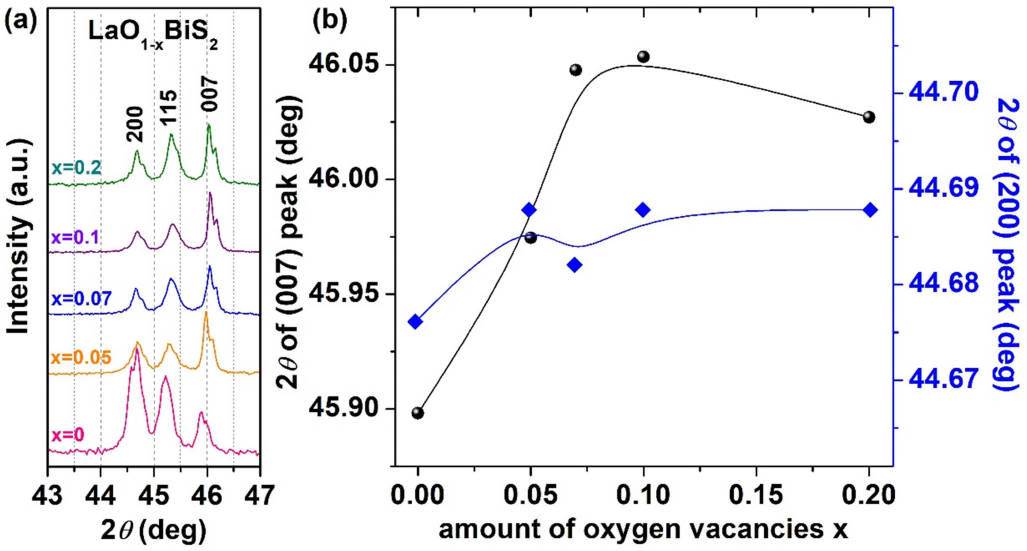

Fig. S1 (a) Enlarged XRD patterns of polycrystalline $LaO_{1-x}BiS_2$ with x = 0, 0.05, 0.07, 0.1, 0.2. (b) Positions of the (007) and (200) XRD diffraction peaks as a function of x, reflecting to the lattice constants of a and c for the tetragonal unit cell, the solid lines are guides to the eyes.

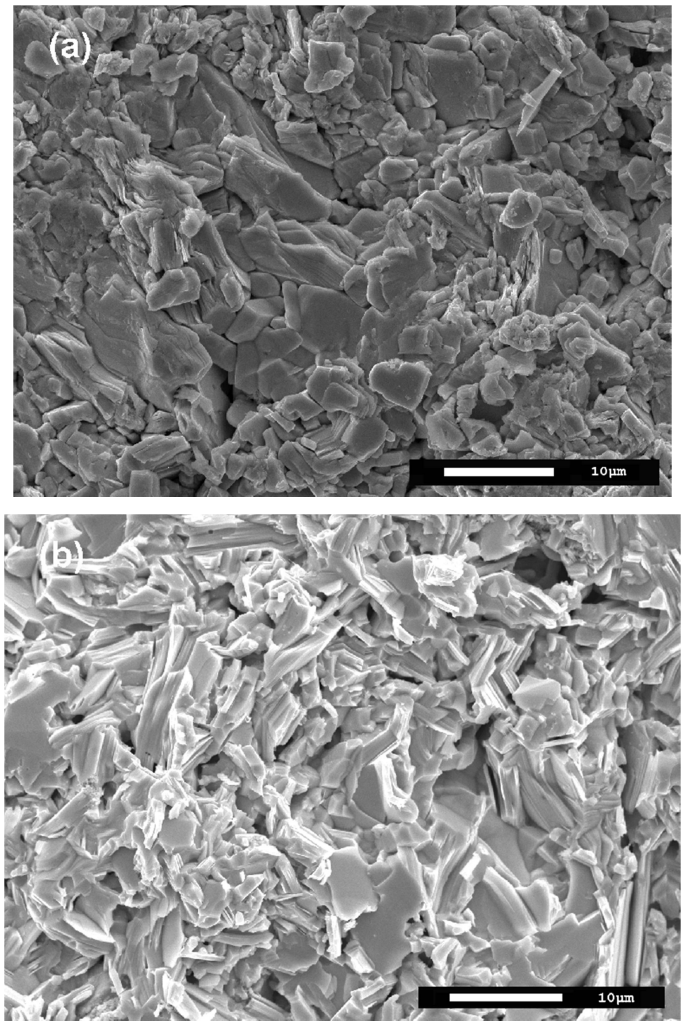

Fig. S2 SEM micrographs of polycrystalline (a) parent sample $LaOBiS_2$ and (b) $LaO_{0.93}BiS_2$, the distinct difference of SEM micrographs between $LaOBiS_2$ and $LaO_{0.93}BiS_2$ is observed, parent sample $LaOBiS_2$ shows grain-shaped crystals with a few slice-shaped ones, and $LaO_{0.93}BiS_2$ sample show well oriented slice-shaped crystals.

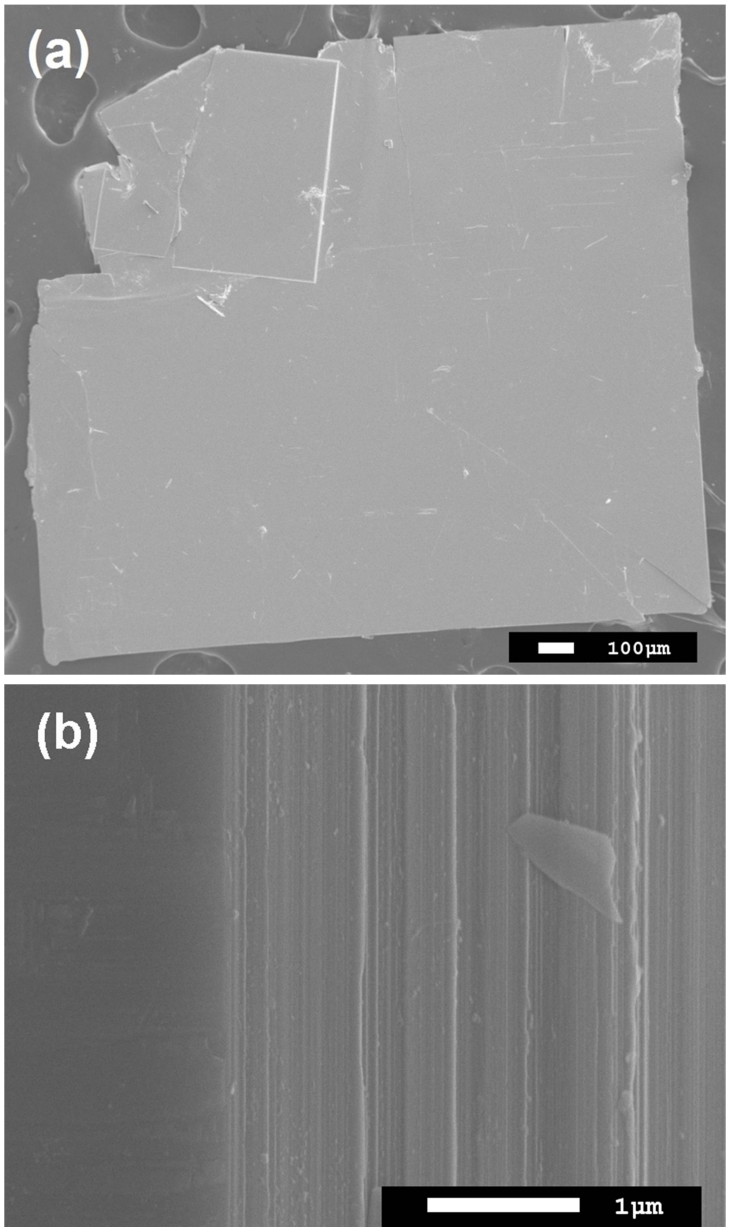

Fig. S3 SEM micrograph of single-crystalline $LaO_{0.93}BiS_2$, (a) image of an as-synthesized single crystal with a plate-like shape and smooth surface, the typical size is about 2mm. (b) SEM micrograph of crystal profile, obvious layered structure can be observed.

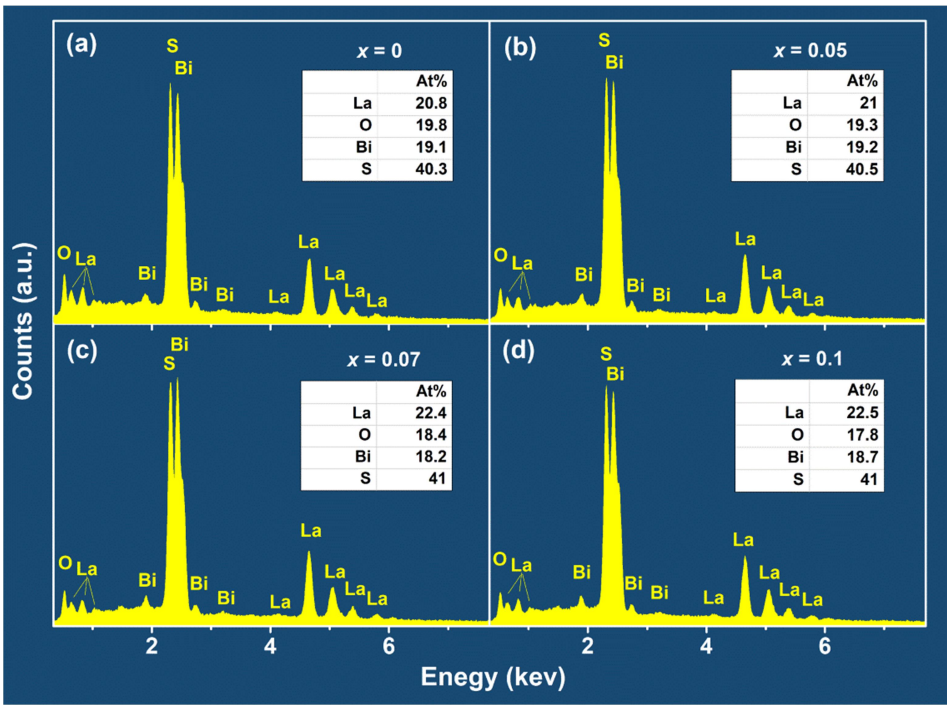

Fig. S4 EDS spectrum of synthesized polycrystalline samples $LaO_{1-x}BiS_2$ with (a) $x = 0$, (b) $x = 0.05$, (c) $x = 0.07$, (d) $x = 0.1$. Inset in each figure shows atomic percentage (At%) of La, O, Bi, S in sample, which is so close to the nominal composition. However, the actual oxygen content in polycrystalline sample with $x = 0.2$ obviously deviates from the nominal composition, due to the appearance of impurity phase (not show here).

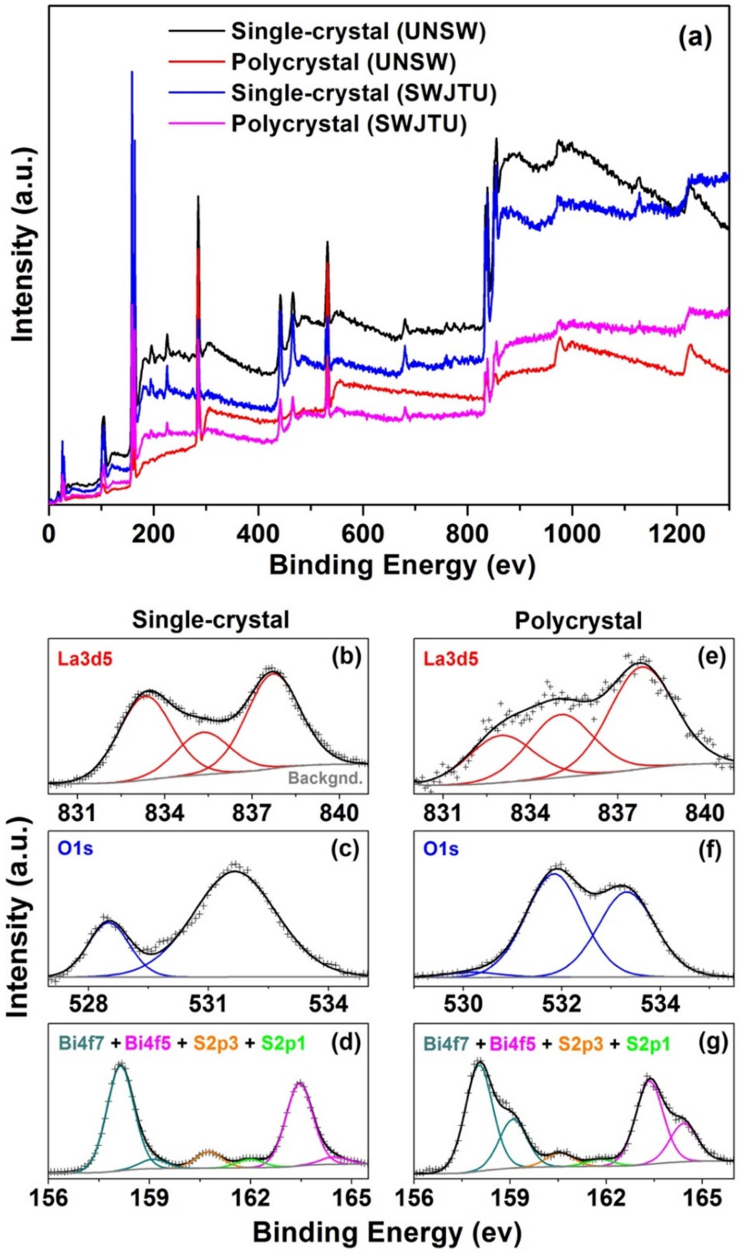

Fig. S5 (a) The XPS survey spectra for polycrystalline and single-crystalline $LaO_{0.93}BiS_2$ samples were taken at SWJTU and UNSW, respectively. (b)-(g) high resolution XPS spectra and peak fitting in the narrow range of the binding energy for La3d, O1s, Bi4f, and S2p, respectively.

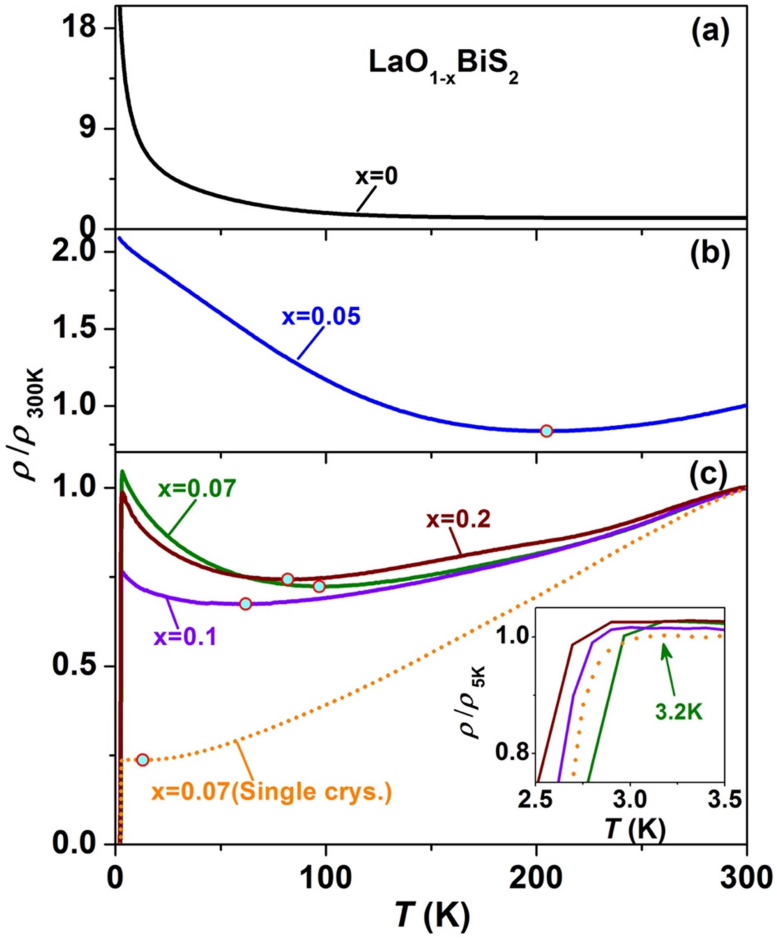

Fig. S6 The temperature dependence of the normalized electrical resistivity of $LaO_{1-x}BiS_2$ with different oxygen vacancy content, solid lines for polycrystalline samples, and dot line for single-crystalline sample. (a) parent phase $LaOBiS_2$, (b) polycrystalline $LaO_{1-x}BiS_2$ with x = 0.05, (c) polycrystalline $LaO_{1-x}BiS_2$ with x = 0.07, 0.1, 0.2, and single-crystalline $LaO_{0.93}BiS_2$ with current flowing in *ab* plane, inset is enlarged curves around superconducting transition. A sharp drop of ρ/ρ_{5K}(T) was observed at 3.2K for x = 0.07.

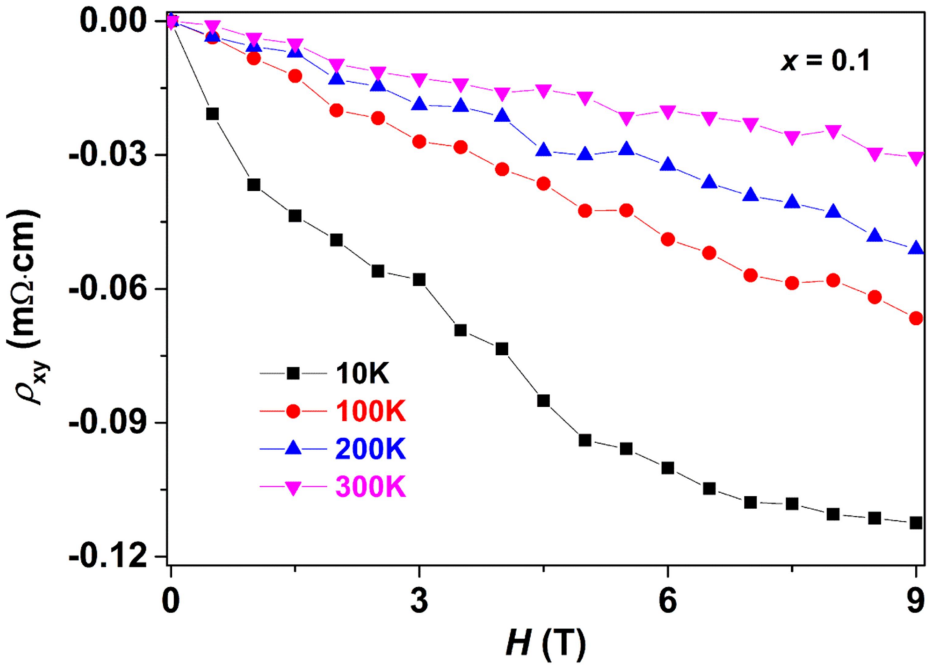

Fig. S7 The Hall resistivity ρ_{xy} vs the magnetic field H at 10, 100, 200, and 300 K for the sample $LaO_{1-x}BiS_2$ with x = 0.1. Negative Hall resistivity ρ_{xy} indicates the electronic charge carriers are the domination one.

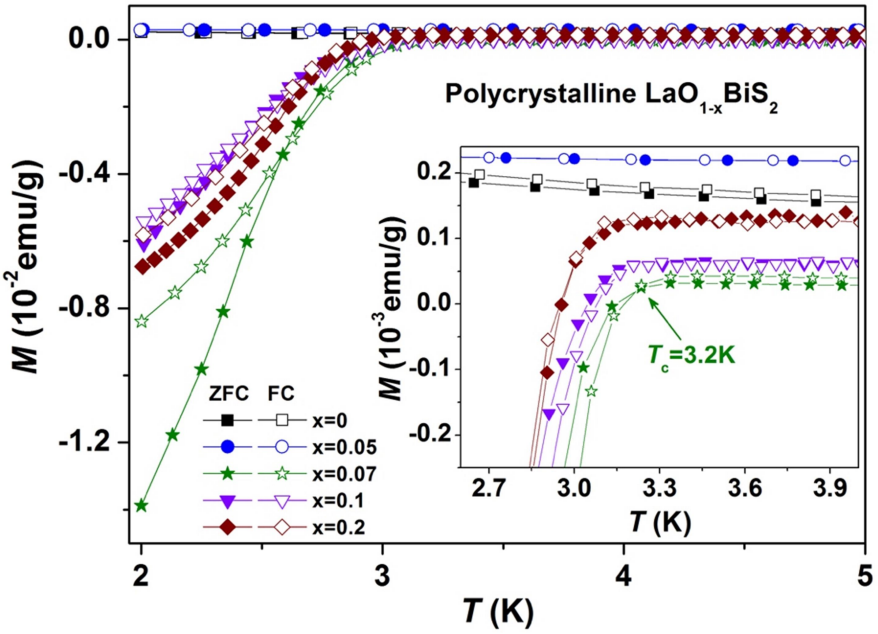

Fig. S8 The temperature dependence of DC magnetization $M(T)$ of polycrystalline $LaO_{1-x}BiS_2$ with x = 0, 0.05, 0.07, 0.1, 0.2, in zero-field-cooling (ZFC) and field-cooling (FC) processes at a magnetic field H of 10Oe. Inset is enlarged view around superconducting transition. Superconducting transition temperatures (T_c) were consistent with the resistivity measurement.

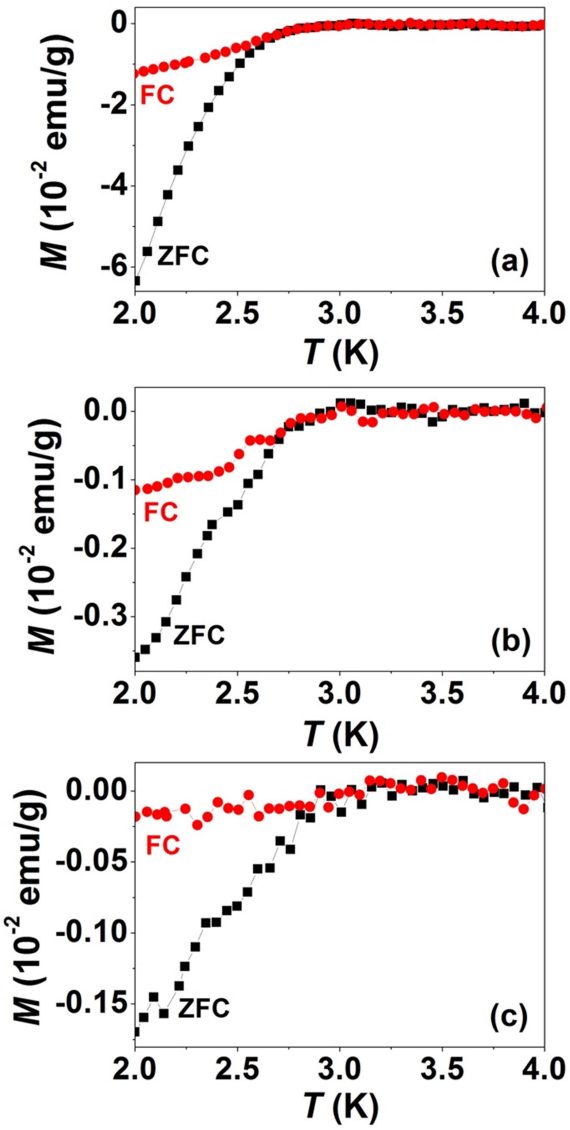

Fig. S9 The temperature dependence of DC magnetization of single-crystalline $LaO_{1-x}BiS_2$ with x=0.07 in ZFC and FC processes at a magnetic field H (//c) of 5Oe , (a) Sample 1, (b) Sample 2, (c) Sample 3.

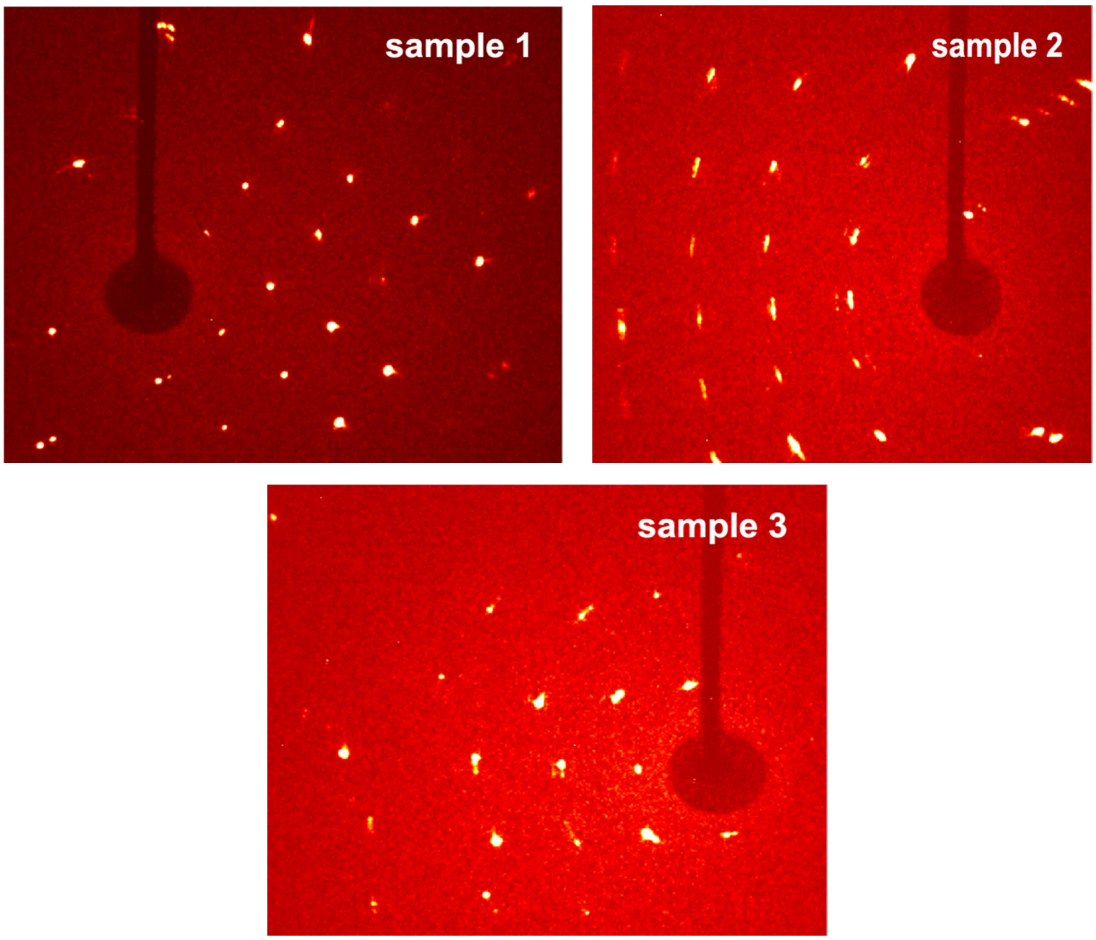

Fig. S10 X-ray diffraction images of Sample 1, Sample 2, and Sample 3. The diffraction spots of Sample 1 and 3 are sharper than Sample 2, and that of Sample 2 shows streaked, maybe indicate a small amount of defects or local strain exist in Sample 2.

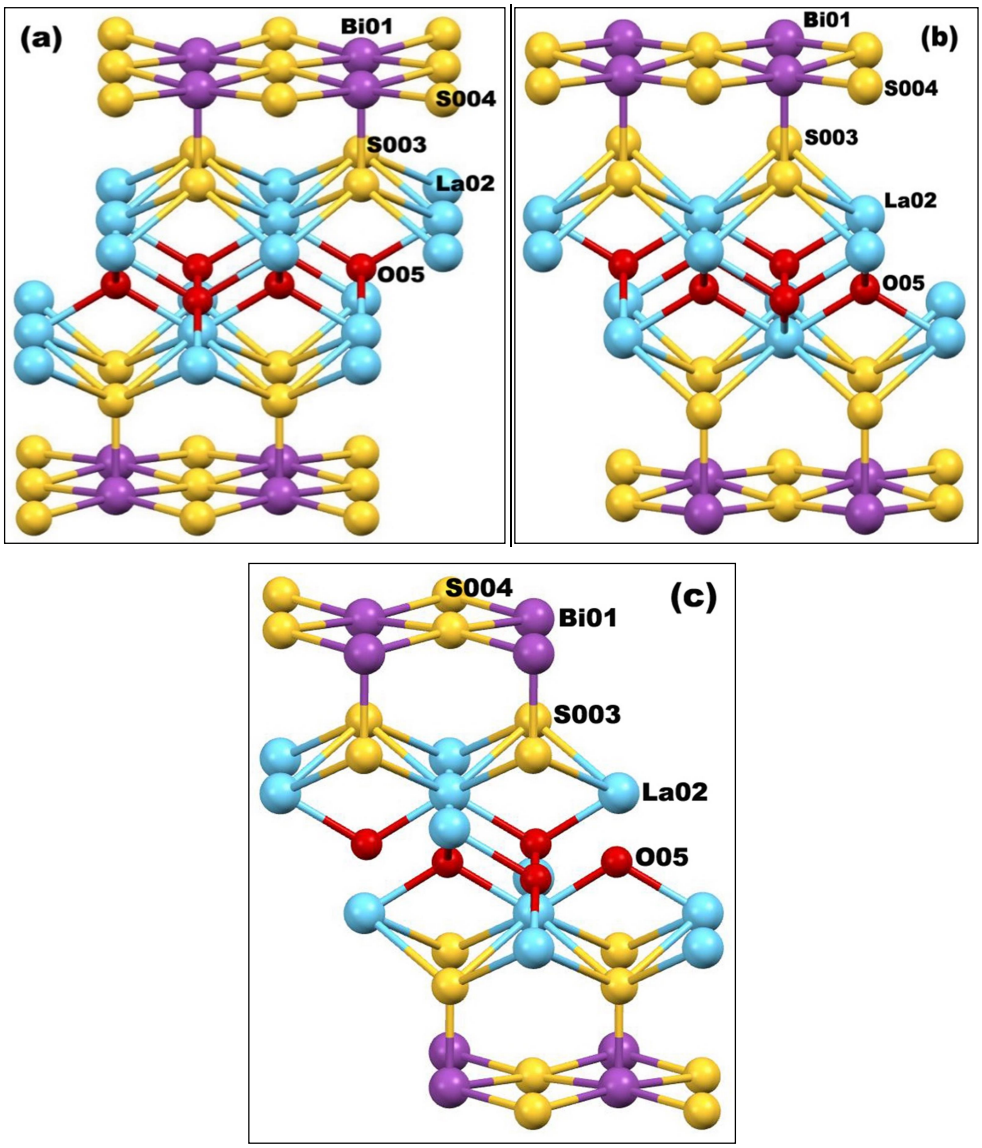

Fig. S11 Crystal structures of single-crystalline $LaO_{1-x}BiS_2$ with x = 0.07, consist of BiS_2 bilayers sandwiched between La_2O_2 blocking layers. The Bi ions coordinated by four in-plane (S004) and one out-of-plane (S003) sulfur ions. (a) Sample 1, (b) Sample 2, (c) Sample 3.

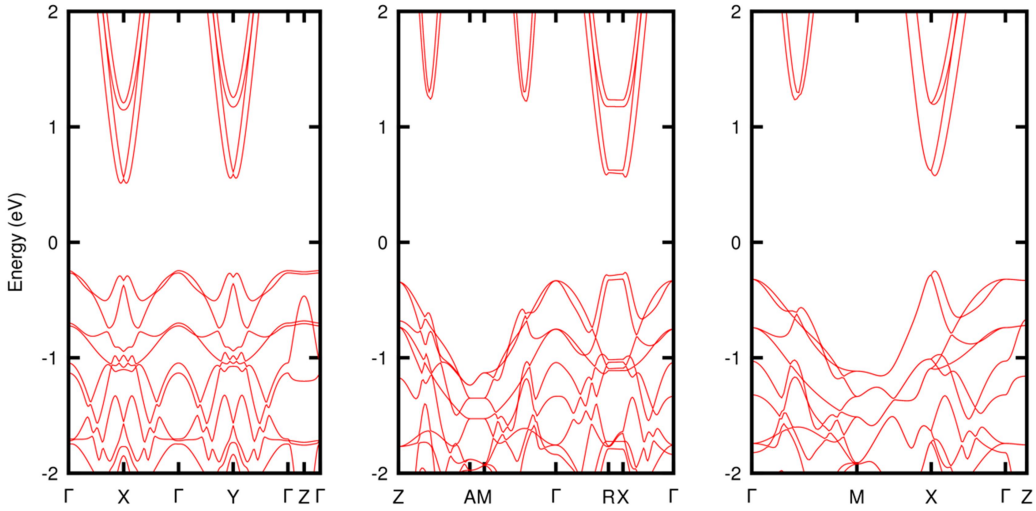

Fig. S12 Band structure of the pristine structure of $LaOBiS_2$ corresponds to the $P\ \bar{1}$, $P2_1/m$, *P4/nmm* (*P4/n*) space groups respectively (from right). The calculations were done with the spin-orbit effect.

Table S1 Refined atomic coordinates (x, y, z), selected interatomic distances (Å) and angles (deg) in $LaO_{0.93}BiS_2$ determined by single-crystal X-ray diffraction analysis.

	Sample 1	Sample 2	Sample 3
Atom	(x, y, z)	(x, y, z)	(x, y, z)
Bi01	0.25, 0.25, 0.12888(11)	0.2510(5), 0.7500, 0.12929(18)	0.2487(3), 0.7495(3), 0.12901(10)
La02	0.75, 0.75, 0.40825(17)	0.7482(7), 0.2500, 0.4081(3)	0.7507(4), 0.2515(5), 0.40880(16)
S003	0.25, 0.25, 0.3101(7)	0.261(3), 0.7500, 0.3116(12)	0.2478(16), 0.7459(18), 0.3096(6)
S004	0.75, 0.75, 0.1171(9)	0.744(3), 0.2500, 0.1164(15)	0.7558(19), 0.257(2), 0.1185(8)
O05	1.25, 0.75, 0.50	0.762(9), 0.7500, 0.495(3)	0.754(6), 0.761(6), 0.500(2)
Distances (Å)			
Bi01-S003	2.50	2.51	2.485(8)
Bi01-S004(1)	2.8720	2.892	2.865(8)
Bi01-S004(2)	-	2.852	2.836(8)
La02-S003(1)	3.171	3.13	3.176(7)
La02-S003(2)	-	3.20	3.158(7)
La02-O05(1)	2.390	2.35	2.36(3)
La02-O05(2)	-	2.47	2.37(3)
La02-O05(3)	-	2.39	2.40(3)
Angles (deg)			
S003-Bi01-S004(1)	93.2	93.0	93.1(2)
S003-Bi01-S004(2)	-	94.1	92.7(2)
S004-Bi01-S004(1)	89.8	89.8	88.7(3)

S004-Bi01-S004(2)	173.5	172.9	174.0(3)
S004-Bi01-S004(3)	-	90.5	90.9(3)
S004-Bi01-S004(4)	-	88.9	89.3(3)
S003-La02-O05(1)	140.2	142	140.3(6)
S003-La02-O05(2)	71.5	71	71.3(6)
S003-La02-O05(3)	140.2	140	138.4(6)
S003-La02-O05(4)	-	72.5	71.4(6)
S003-La02-S003(1)	129.5	130.2	129.0(2)
S003-La02-S003(2)	79.5	80.8	79.8(2)
S003-La02-S003(3)	-	79.8	79.6(2)
S003-La02-S003(4)	-	78.7	78.7(2)
O05-La02-S003 (1)	-	142	141.6(6)
O05-La02-S003 (2)	-	138	140.9(6)
O05-La02-S003 (3)	-	70	71.0(6)
O05-La02-O05(1)	116.1	119	116.6(9)
O05-La02-O05(2)	73.73	75	74.6(9)
O05-La02-O05(3)	-	72	75.8(9)
Bi01-S003-La02(1)	115.3	115.8	115.3(3)
Bi01-S003-La02(2)	-	114.0	115.0(3)
La02-O05-La02(1)	116.08	119	117(1)
La02-O05-La02(2)	106.27	108	105(1)